Powder Technology 300 (2016) 46–60

Contents lists available at ScienceDirect

Powder Technology

journal homepage: www.elsevier.com/locate/powtec

# Three dimensional characterization of morphology and internal structure of soft material agglomerates produced in spray fluidized bed by X-ray tomography

R. Pashminehazar *, A. Kharaghani *, E. Tsotsas

*Thermal Process Engineering, Otto von Guericke University Magdeburg, Universitätsplatz 2, Magdeburg 39106, Germany*

ARTICLE INFO

*Article history:*
Received 3 September 2015
Received in revised form 21 March 2016
Accepted 30 March 2016
Available online 1 April 2016

*Keywords:*
Spray fluidized bed agglomeration
Amorphous maltodextrin
X-ray micro-computed tomography
Microstructural characterization
Morphological descriptors

ABSTRACT

Food powders such as maltodextrin are often produced in agglomerate form in spray fluidized beds in order to enhance their user properties. These agglomerates mostly have complex structures and irregular shapes. The internal structure and morphology of food agglomerates have rarely been investigated at the microscopic scale. In this work, a nondestructive X-ray micro-computed tomography technique is used as an appropriate experimental method to overcome this lack of data by a thorough characterization of the three-dimensional internal structure of maltodextrin agglomerates. A sequence of image processing steps is applied to the X-ray images in order to obtain 3D views and to extract data for the morphological characterization. The internal porosity as well as the size and spatial distribution of the pores inside the agglomerates are evaluated. Open pores formed during the agglomeration process are also determined from the X-ray images. The agglomerate shape is investigated and compared by 2D and 3D image analyses. Maltodextrin primary particles with non-spherical shape have a broad size distribution, and they may deform and overlap as they go above the glass transition temperature during the agglomeration process. A comprehensive methodology is developed based on the preflooded watershed segmentation of X-ray images to distinguish the primary particles in maltodextrin agglomerates. On this basis, the radius of gyration and the fractal dimension are calculated. A low fractal dimension of 1.8 is found, which proves that the structure of maltodextrin agglomerates is more open and fluffier than the structure of insoluble hard material agglomerates.

© 2015 Elsevier B.V. All rights reserved.

## 1. Introduction

In various industries fine powders are produced in agglomerated form in a fluidized bed in order to improve their flowability, instant properties or simply to improve the optical appearance of the product [1]. Fluidized bed agglomeration is a complex process with many interdependent factors that influence the quality of the end product. In spray fluidized bed agglomeration, the primary particles are fluidized by blowing hot air from the bottom of the granulator, while a binder solution or suspension is sprayed as small droplets onto the particles, creating liquid bridges, which finally lead to agglomerates. Our understanding of the physical phenomena that occur during spray fluidized bed agglomeration has been significantly enhanced by recently developed Monte Carlo simulation [2] and population balance models [3]. Despite this progress, it still remains a challenge to characterize the structure of agglomerates (especially food agglomerates) produced in a spray fluidized bed. A successful characterization should allow a better understanding of process–structure or structure–property relationships. The quantification of the internal microstructure of agglomerates is also crucial for setting up processing maps and for describing agglomeration patterns and mechanisms.

Most of the food, pharmaceutical and chemical powders which are agglomerated are water-soluble. Maltodextrin may serve as a model substance for many amorphous-water soluble food powders. Agglomeration of this kind of material, which has a low glass transition temperature, is more difficult due to the strong adhesive forces between moist amorphous particles. This leads to a rather broad particle size distribution and to the formation of a crust on the equipment surface and around the spraying nozzle [1].

Several studies were performed on the effect of process parameters such as fluidizing air flow rate, temperature, agglomeration time and binder spray rate on the growth kinetics of maltodextrin agglomerates, and on their physical, mechanical and rheological properties [4–6]. Moreover, in recent publications on the agglomeration of amorphous material, the fluid, particle and collision dynamics inside a fluidized bed granulator was described in detail using coupled DEM–CFD simulations. Different process variables and granulator configurations (i.e., top spray, Wurster coater, spouted bed) were compared in terms of the agglomeration probability, the breakage and growth rate as well as the agglomerate strength [7,8].

* Corresponding authors.
*E-mail addresses:* reihaneh.pashminehazar@ovgu.de (R. Pashminehazar), abdolreza.kharaghani@ovgu.de (A. Kharaghani).

http://dx.doi.org/10.1016/j.powtec.2016.03.053
0032-5910/© 2015 Elsevier B.V. All rights reserved.

**Nomenclature**

| | |
|---|---|
| $A$ | area [$m^2$] |
| $C$ | circularity [−] |
| $d_A$ | equivalent projected area diameter of primary particle [m] |
| $d_{FeMin}$ | minimum Feret diameter of primary particle [m] |
| $d_V$ | equivalent volume diameter of primary particle [m] |
| $D_f$ | fractal dimension [−] |
| $D_{FeMin}$ | minimum Feret diameter of agglomerate [m] |
| $I_G$ | mass moment of inertia [kg $m^2$] |
| $k_g$ | fractal pre-factor |
| $M$ | mass [kg] |
| $N_p$ | number of primary particles in agglomerate [−] |
| $P$ | perimeter [m] |
| $r$ | radial coordinate [m] |
| $r_G$ | position vector of center of mass [m] |
| $r_i$ | position vector of primary particle center [m] |
| $\bar{r}_p$ | mean radius of primary particles [m] |
| $R_e$ | equivalent radius [m] |
| $R_g$ | radius of gyration [m] |
| $S$ | surface area [$m^2$] |
| $V_{agg}$ | total volume of agglomerate [$m^3$] |
| $V_b$ | bulk volume [$m^3$] |
| $V_{cp}$ | volume of closed pores |
| $V_s$ | volume of compact solid phase in agglomerate [$m^3$] |
| $V_{s,cp}$ | volume of solid phase including internal pores in agglomerate [$m^3$] |

*Greek letters*

| | |
|---|---|
| $\varepsilon_b$ | bulk porosity [−] |
| $\varepsilon_{cp}$ | porosity of closed pores [−] |
| $\varepsilon_{op}$ | porosity of open pores [−] |
| $\rho$ | mass density [kg/m] |
| $\phi_S$ | sphericity [−] |

The physical properties of a material are strongly influenced by its internal microstructure, which is created during processing [9]. Despite the amount of research on maltodextrin agglomeration, the internal microstructure and morphology of this kind of agglomerates have rarely been investigated, especially in three dimensions. Most of the available studies were performed with non-soluble particles and only a few of them investigated the microstructure of particles undergoing glass transition [10,11]. The first systematic studies on various morphological descriptors for fluidized bed agglomerates were published by Dadkhah et al. [12] for hard non-porous and porous primary particles (glass beads and $\gamma$-$Al_2O_3$, respectively). The primary particles in [12] are insoluble in the binder, however the maltodextrin is amorphous material that can absorb water and deform during agglomeration. The methodology and image processing sequences developed in [12] are merely effective for agglomerates made from primary particles which do not deviate too much from the spherical shape. Whereas, the methodology developed in this work can be used for agglomerates with irregular shape.

Common analytical techniques applied to the study of agglomerate microstructure are restricted to two-dimensions. The advantage of these techniques is that they provide rather inexpensive and rapid quantitative analysis. The drawback is that the sample preparation for such techniques is often destructive and the techniques do not provide direct information in the third dimension. Therefore, such 2D data may not fully represent the true 3D structures [13]. X-ray micro-computed tomography (μ-CT) on agglomerate specimens provides an opportunity to completely analyze the structure of the sample in three dimensions. X-ray μ-CT is a nondestructive 3D imaging technique which uses a set of two-dimensional shadow X-ray images of an object to reconstruct its three-dimensional structure using a mathematical algorithm [14].

In this study, suitable process parameters were determined for the production of maltodextrin agglomerates in a spray fluidized bed. In two-dimensional analyses, the size and shape of the primary particles and of the agglomerates were studied with a Camsizer. The results are presented as the evolution of the median diameter, particle size distribution and circularity. The microstructure of individual agglomerates (obtained by X-ray micro tomography) is visualized down to details that contain valuable information such as the actual morphology and spatial distribution of primary particles and pores, which cannot be assessed by other techniques. By further processing of the X-ray image sequences, the micro-scale morphology of soft agglomerates made of maltodextrin particles is studied and the results are evaluated quantitatively. The internal porosity and the pore size distribution of the primary particles as well as of the agglomerates are obtained and evaluated. The open pores of agglomerates, which comprise relatively large cavities and channels, are also determined from the X-ray images. The open porosity of agglomerates is calculated by three different methods, i.e. convex hull, dilation and radius of gyration, and the results are compared. The bulk porosity is also measured for maltodextrin particles before and after agglomeration. The shape of the agglomerates is analyzed in terms of sphericity and compared with two-dimensional values. Moreover, a comprehensive methodology is developed based on the segmentation method using preflooded watershed transform to distinguish and separate the primary particles in maltodextrin agglomerates. The gyration radius and fractal dimension of agglomerates are also calculated based on the separated primary particles.

## 2. Materials and experimental methods

### 2.1. Spray fluidized bed agglomeration

In order to obtain a narrow size distribution of primary particles used in the agglomeration process, maltodextrin powder (DE 12, Glucidex, Roquette, France) was sieved in the range of 300 to 500 μm. The agglomeration was performed in a lab-scale batch fluidized bed granulator (GPCG 1.1 LabSystem) with a transparent, cylindrical fluidization chamber made of Plexiglas with 152 mm inner diameter and 450 mm height (Glatt GmbH, Germany). For amorphous polar (water-soluble) powders it is mostly sufficient to atomize water on the fluidized particles [1]. Therefore, pure water was sprayed as a binder (plasticizing agent) with a two-fluid nozzle (model 940) provided by Düsen-Schlick GmbH (Untersiemau, Germany). The nozzle was placed on top of the chamber at the height of 150 mm from the distributor plate and operated with relative air pressure of 0.5 bar. For each experiment, 50 g of powder was fluidized using a constant fluidization air flow rate of 70 kg/h, heated by an electrical heater up to 50 °C before it enters into the chamber. The temperature sensor was located below the distributor plate. The maltodextrin powder was preheated before spraying the water. With a piston pump the water was sprayed at a constant rate. The process parameters for agglomeration are summarized in Table 1. The total agglomeration time was about 5 min and after that a sample

**Table 1**
The values of process parameters used for the agglomeration of maltodextrin DE 12.

| Parameter | Value |
|---|---|
| Primary particle diameter (μm) | 300–500 |
| Bed hold up mass (g) | 50 |
| Air flow rate (kg/h) | 70 |
| Inlet air temperature (°C) | 50 |
| Binder spraying rate (g/min) | 1.75 |
| Atomization air pressure (bar) | 0.5 |

was taken using a sampling tube which was located in the lower part of the bed. Particle size distribution and circularity of the primary particles and agglomerates were measured simultaneously by a Camsizer that uses the principle of dynamic digital image analysis (Retsch Technologies GmbH, Germany). For each measurement, the projected particle shadows were recorded at a rate of more than 60 images per second. In this way, every single particle of the sample was recorded and evaluated in a short time. With the used device, it was possible to measure a wide range of particle sizes (30 μm–30 mm) with a resolution capacity in the micrometer range.

### 2.2. X-ray micro-computed tomography exposure setting

The internal microstructure of agglomerates was determined from the 3D reconstructed images using an X-ray micro-computed tomography device (CT Procon alpha 2000, manufactured by ProCon X-ray GmbH, Germany). Each agglomerate was scanned individually within the entire range of 0–360° with a rotation step of 0.3°. Typically, each measurement required a long time of around 2 h. Therefore, a limited number of agglomerates (between 20 and 25) were selected and scanned. The samples were picked randomly to cover a wide range of agglomerate sizes in the bed. These agglomerates were neither very small nor clumped together.

The agglomerate was placed on a sample holder and rotated to obtain radiographic projections from different angles. X-rays passing through the material are absorbed according to a linear attenuation coefficient that has some spatial variation depending on the average atomic number, density and thickness of the material. Sufficient data obtained from the projection images was recorded by a 2D panel detector of 2048 × 2048 pixels to reconstruct slices of the three-dimensional object. In order to obtain images with sufficient contrast and resolution from which the structural constituents can easily be separated, the X-ray source was set at 50 kV and 110 μA. The distance between detector and X-ray beam source was 380 mm, and the sample was located between them at distance of 8 mm away from the X-ray tube. This parameter setting led to a voxel edge length of 2.2 μm. Three images were taken per angular position, with an exposure time of 1500 ms.

### 2.3. Image processing

In order to obtain data required for morphological analysis, different steps of image processing need to be performed on the X-ray images. The conducted image processing steps were as follows. At first, the volume of interest was extracted. This volume was considered as the part of the image containing the agglomerate on which the image analysis was performed. Then, segmentation (binarization) was performed for separating the pixels of the gray-scale images into background and foreground. Based on Otsu's thresholding method [15] a binary image was created: the value 1 (white) was assigned to all the pixels with intensity higher than the given gray tone value (threshold), while the value 0 (black) was assigned to the other pixels, i.e. pores and background. Before further analysis, all images were smoothed with a median filter to eliminate noise. Sample holder effects were removed by labeling and object filtering method. Finally, the volume image and internal microstructure of agglomerates were visualized. The qualitative and quantitative analyses were performed on these binary volume images. For basic image processing steps the MAVI software developed by Fraunhofer Institute for Technical and Industrial Mathematics in Kaiserslautern, Germany, was used. For further analysis (i.e. separating primary particles, calculating porosity and sphericity, visualization of particles and pores) additional image processing operations combined with both Matlab (version R2012b) code and its Image Processing Toolbox are necessary.

## 3. Evaluation methods

### 3.1. Primary particle separation

Separation and distinction of the primary particles comprised in an agglomerate are an important and challenging issue for analyzing the morphology of the agglomerate. When the primary particles are spheres or have some other well-defined shapes, it is much easier to distinguish them in the agglomerate structure. Amorphous materials such as maltodextrin have an a priori unknown shape and structure. Moreover, the structure deforms during the agglomeration process because of water absorption, mostly at the contact points between the primary particles.

In this study, the separation of primary particles in agglomerate is done by segmentation of X-ray images using the preflooded watershed method. Applying the watershed method without considering limitations that can be checked by separate measurement may not, though, yield reasonable results.

The process of separating objects from the image background, as well as from each other is called segmentation. There are many different ways to perform image segmentation. Segmentation methods for identifying and separating foreground regions include labeling and the watershed transformation. The input data for labeling is a binarized image, whereas the watershed transformation requires a gray-level image. After labeling, the output image contains discrete label values for each pixel, identifying connected regions. Therefore, the labeling method is not applicable for separating the primary particles of agglomerate, as these are connected objects.

The watershed transformation is a more complex and powerful morphological technique for image segmentation [16,17]. The basis of watershed is topographic representation of a gray-level image, which includes three basic notions: minima, catchment basins and watershed lines. Imagine the bright areas to have “high” altitudes and the dark areas to have “low” altitudes. Suppose that there is a hole in each local minimum through which water can flow out with a constant flux and that when two basins merge, a dam is built: the set of all dams defines the so-called watershed lines. Such lines represent the watershed boundaries that are good indicators for feature partitioning [16–18]. During this process, watershed lines get the label 0, whereas each basin is assigned a specific label different from 0. Usually, the standard morphological watershed transformation applied to gray-value images results in strongly over-segmented images. Over-segmentation occurs because every regional minimum, even if small and insignificant, forms its own catchment basin. It can be somewhat improved by filtering, but this does not solve the problem completely. To decrease the over-segmentation of watershed-based techniques, several approaches have been proposed in the literature [16,18]. General strategies to avoid over-segmentation are pre-processing, modification and post-processing of the image.

A modification with straightforward interpretation to overcome over-segmentation is the volume preflooded watershed algorithm, in which basins with a volume below a specified value are merged with neighboring basins during the watershed process [19]. The algorithm is altered in the following way: During the flooding of the image, at each step the pixels of the created basins are counted. If their number is larger than a specified minimum, a new basin is created with a watershed line. If the number of pixels is below the value, however, then the basin is discarded and thus prevented from creating watersheds. In this case, it will be integrated into a bigger basin.

The maltodextrin agglomerates produced in this work are highly porous and also the differences in gray value between air and substance are not very large, due to the low density of maltodextrin. Therefore, the gray-level images exhibit some noise in pores and in the air surrounding the agglomerate. Although by the volume preflooded watershed method the over-segmentation is reduced, some unwanted segmentation still appears in the surrounding area. Since only a

separation of the primary particles in the agglomerates is required, an additional step is used to eliminate the segmentation of the air phase.

In order to eliminate the noise and to smoothen the image properly, it is binarized first by thresholding segmentation. In this case only the solid material gets the label 1 (foreground) and the surrounding area gets the label 0 (background). As mentioned before, gray-value images are required for the watershed transformation in order to find the minimal values. In this regard, a Euclidean distance transform is applied to the binarized X-ray images. This transformation computes the absolute or squared Euclidean distance of each background pixel to the closest foreground pixel. It produces a gray-value image of the same size as the original image. Then, by using the preflooded watershed transformation on this image the segmentation and partitioning of the system occur only for the agglomerate. Therefore, when combined with the Euclidean distance transformation, the preflooded watershed can be used for the separation of connected primary particles of an agglomerate. It should be noted that the minimal number of pixels in preflooded watershed should be defined properly in order to have a reasonable separation procedure.

Using the data extracted from the volume images after segmentation, the primary particles can be labeled and counted, providing the number $N_p$ of primary particles in each agglomerate. The center coordinates, volume and surface area of each primary particle can also be identified.

### 3.2. Gyration radius

The gyration radius, $R_g$, is one of the basic properties for characterizing an agglomerate. The moment of inertia, $I_G$, of a body is often defined in terms of its radius of gyration, which is the radius of a ring of equal mass, $M$, around the center of mass of a body that has the same moment of inertia. Therefore, the radius of gyration is:

$$I_G = MR_g^2 \rightarrow R_g = \sqrt{\frac{I_G}{M}}. \tag{1}$$

The radius of gyration describes not only the size of an object, but also shows how the mass is distributed around the center of gravity. Two objects with the same mass or volume may have different radii of gyration, in which a lower value indicates that the mass of the object is distributed more uniformly around the center of gravity.

In polymer science the radius of gyration is calculated as:

$$R_g^2 = \frac{1}{N_p}\sum_{i=1}^{N_p}(r_i - r_G)^2 \tag{2}$$

where $N_p$ is the number of monomers or (in the present case) primary particles, $r_i$ is the position vector of each primary particle and $r_G$ is the position vector of the object's center of mass. The following formula is also useful [20]:

$$R_g^2 = \frac{1}{2{N_p}^2}\sum_{i=1}^{N_p}\sum_{j=1}^{N_p}(r_i - r_j)^2. \tag{3}$$

It indicates that one can use the mean squared distances between all pairs of primary particles to obtain $R_g$, instead of first calculating $r_G$ and then the mean square distance between $r_G$ and each primary particle [12,20]. In this study, each separated primary particle of the agglomerate is considered as a sphere with the volume and center coordinates of the actual primary particle (Fig. 1). As we have the center coordinates of each primary particle, the radius of gyration can be calculated for different agglomerates. Without having 3D data, the determination of the radius of gyration is practically impossible.

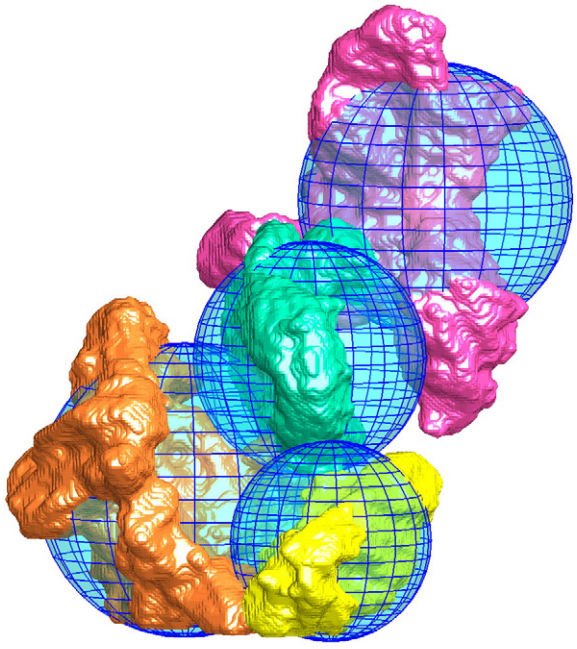

**Fig. 1.** Spherical representation model for an agglomerate with separated primary particles.

### 3.3. Porosity

The porosity can be defined based on the size and gray value of the pixels comprised in a volume image obtained from the X-ray μ-CT method. Mathematical morphology is a powerful tool for geometrical analysis and description, which contains a broad set of operations that process images based on shapes. All morphological operators take two pieces of data as their input. One is the input image, which may be either binary or gray scale for most of the operators. The other is the structuring element, which determines the precise details of the effect of the operator on the image. Morphological operations apply a structuring element to an input image, creating an output image of the same size. In a morphological operation, the value of each pixel in the output image is based on a comparison of the corresponding pixel in the input image with its neighbors. By choosing the size and shape of the neighborhood by structuring elements, a suitable morphological operation that is sensitive to specific shapes in the input image can be constructed. Different types of porosity are used in food process design and for food product characterization [21]. These are discussed in the following sections.

#### 3.3.1. Porosity of closed pores (internal porosity)

The closed porosity is defined as the ratio of the inner pore volume inside the compact solid material, $V_{cp}$, to the volume of solid phase, including internal pores in the agglomerate, $V_{s,cp}$. This porosity is mostly attributed to the primary particle structure and is defined as:

$$\varepsilon_{cp} = \frac{V_{cp}}{V_{s,cp}} = 1 - \frac{V_s}{V_{s,cp}}. \tag{4}$$

The volume of the compact solid phase in the agglomerate, $V_s$, can be obtained directly from a binary image, however further image processing is required in order to obtain $V_{s,cp}$. An example of this procedure is shown in Fig. 2.

To calculate the total volume of the solid phase, including internal pores in the agglomerate, the internal pores should be filled. For this purpose, the mathematical morphology operation of closing can be performed on the volume images obtained by μ-CT. Closing is an operator that enlarges the boundaries of foreground regions in an image and

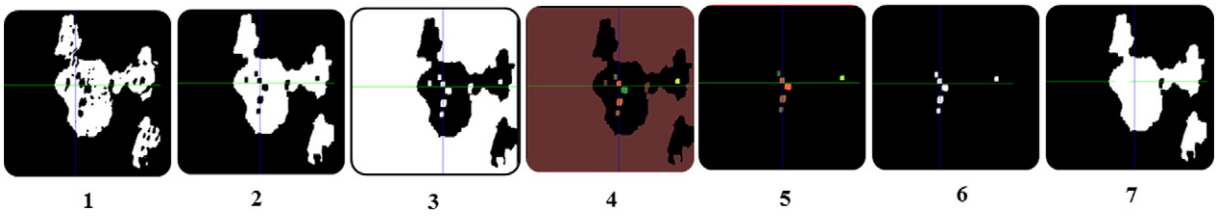


**Fig. 2.** Image processing sequences applied for filling the internal pores and for calculating the volume of the solid phase including internal pores in the aggregate, $V_{s,cp}$: (1) binary image, (2) closing morphology (filling small pores), (3) complement (inversion of the images), (4) segmentation-labeling (identification of big pores and surrounding air), (5) object filter (filtering out the surrounding air), (6) binarization, (7) combination of images 2 and 6 (filling of all internal pores). In the first and last images, white pixels belong to the solid phase and black pixels to the air.

shrinks the background, such that small holes within the image are filled (closed). Morphological closing of an image consists of a dilation followed by an erosion operation with the same structuring element. Therefore, it is less destructive than other morphological operations and it preserves the original size, shape and convexity of the analyzed structure. The closing operation requires definition of a structuring element. This structuring element determines the precise effect of the closing operation on the input volume image.

The size and shape of the structuring element should be defined in a way to avoid any remaining unfilled pores within the volume image. Special care should be also taken to control and preserve the exterior surface of the agglomerate. Having performed several tests with different structuring elements, it was observed that the closing method results in an undesired deformation of the exterior surface of the agglomerate, when applied to fill some of the larger internal pores. Therefore, in this work only the small pores were filled with the closing method. This step was used to fill in particular the small pores which were near the exterior surface of the agglomerate and were connected to the surrounding air. After inverting the image in the next step, the air was labeled. In this way, the surrounding air and the larger pores are assigned different labels. After filtering out the surrounding air and after binarizing the images, the larger internal pores of the agglomerate can be filled by adding the corresponding binarized image to that of filled (closed) small pores.

Fig. 2 illustrates the procedure on a two-dimensional slice of the volume image. 3D views of the agglomerate before and after filling its internal pores as well as the internal pore space are shown in Fig. 3. The compact and the total solid phase volume of this agglomerate are $V_s = 5.25 \times 10^{-2}$ mm$^3$ and $V_{s,cp} = 6.63 \times 10^{-2}$ mm$^3$, respectively.

By subtracting Fig. 3a from Fig. 3b, the morphology of the internal pore space becomes accessible (Fig. 3c). After filtering the noise of this volumetric image of pores, the size and spatial distribution of internal pores are obtained.

*3.3.2. Spatial and size distribution of internal pores*

In order to visualize properly the spatial distribution of pores inside the solid phase of the agglomerate, the 3D data matrix of the agglomerate and of its pores is generated individually. In order to achieve this, the original volume image of the agglomerate and its pores – generated by MAVI – is sliced in one spatial direction into a series of 2D binarized images. Then, by using an additionally developed Matlab code, for each slice the spatial coordinates and values of pixels are stored in a 2D matrix. Finally, by combining these 2D matrices the overall 3D matrix is generated.

The size distribution of internal pores is evaluated by the spherical granulometry function. In mathematical morphology, granulometry is an approach to compute the size distribution of grains in binary images, using a series of morphological opening operations. The spherical granulometry assigns to each set of topologically connected pixels the diameter of the largest ball completely contained in the foreground and covering this set of pixels. The granulometric analysis is applied to the 3D μ-CT images of the internal pores and yields a volume-weighted generalized pore size distribution.

*3.3.3. Porosity of open pores*

An open pore is a cavity or channel that is connected to the exterior surface of the agglomerate. The porosity of an open pore is defined as:

$$\varepsilon_{op} = 1 - \frac{V_{s,cp}}{V_{agg}}. \tag{5}$$

For calculating the open porosity, defining the total volume of the agglomerate, $V_{agg}$, is a challenging issue. In this study, three different methods were applied and compared: convex hull, dilation and radius of gyration. The three procedures are illustrated for one small agglomerate in Fig. 4. The gray regions in Fig. 4 are considered as open pore space.

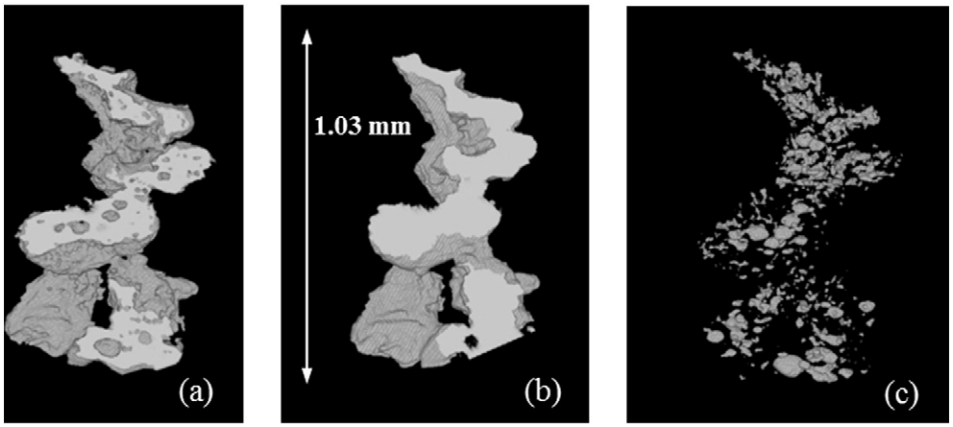


**Fig. 3.** Cross-sectional 3D volume view of agglomerate: (a) before and (b) after filling the internal pores, and (c) internal pore space.

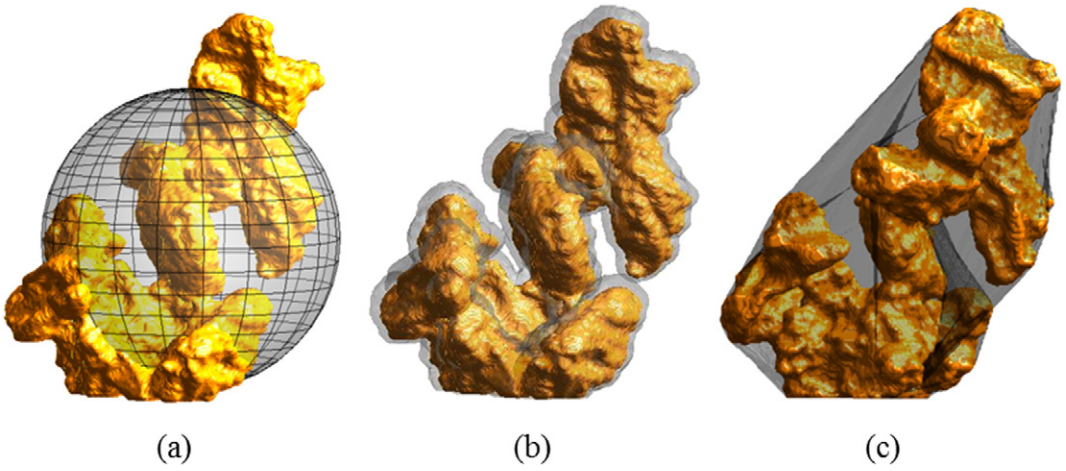


**Fig. 4.** 3D volume views of the same maltodextrin agglomerate for which the total volume is calculated based on three methods: (a) equivalent radius from the radius of gyration, (b) dilation, and (c) convex hull.

*3.3.4. Porosity from the radius of gyration*

The central moment of inertia of a spherical agglomerate with an equivalent radius $R_e$ can be calculated as:

$$I_{mG} = \int_0^{R_e} r^2 dM = \int_0^{R_e} r^2 \rho dV = \int_0^{R_e} 4\pi r^4 \rho dr = \frac{4\pi}{5} R_e^5 \rho \tag{6}$$

where $\rho$ is the apparent density of the agglomerate. At the same time, the mass of the equivalent sphere can be expressed by:

$$M = \frac{4\pi}{3} R_e^3 \rho. \tag{7}$$

Substituting Eqs. (6) and (7) into the definition of the radius of gyration, Eq. (1), the radius of the equivalent sphere, $R_e$, can be expressed as a function of the radius of gyration of the agglomerate, $R_g$:

$$R_e = \sqrt{\frac{5}{3}} R_g. \tag{8}$$

With known radius of gyration, $R_g$, the equivalent radius, $R_e$, and then the total volume of the agglomerate, $V_{agg}$, can be calculated. Inserting $V_{agg}$ in Eq. (5), the agglomerate porosity is obtained.

*3.3.5. Porosity by dilation*

The most basic morphological operations are dilation and erosion. Dilation adds pixels to the boundaries of objects in an image, while erosion removes pixels at object boundaries. The number of pixels added or removed from the objects in an image depends on the size and shape of the structuring element used to process the image. In the morphological dilation and erosion operations, the state of any given pixel in the output image is determined by applying a rule to the corresponding pixel and its neighbors in the input image. In the dilation method, the gray value of any output pixel is the maximum gray value of all the pixels in the neighborhood of the corresponding input pixel. In a binary image, if any of the pixels is set to value 1, the output pixels for all defined neighbors are also set to 1.

In this work, the structuring element with a shape of an approximate ball with a size of 3 pixels was applied to the binary images of individual agglomerates. Setting the volume of the dilated agglomerate equal to the total volume, $V_{agg}$, Eq. (5) can again be used to compute the porosity of open pores.

*3.3.6. Porosity by convex hull*

The convex hull of a set is defined as the smallest convex polygon or polyhedron located in a multidimensional data space which contains all set points (vertices of an object). In the present work the convex hull volume for the 3D image of each agglomerate is calculated by the MAVI software, in which the convex hull is formed by planes perpendicular to the 13 normal directions. By inserting the convex hull volume in Eq. (5), the open pore porosity is obtained. For visualization, the minimal convex hull that envelops the agglomerate is computed for each cross-sectional binary image with the bwconvhull function from Matlab. The three-dimensional reconstruction of the convex hull is done by creating a 3D matrix from all the 2D cross-sectional convex hulls with an additionally developed Matlab code.

*3.3.7. Bulk porosity*

The bulk porosity is the volume fraction of voids outside the boundary of individual particles when packed or stacked [21]. In this study, the agglomerates and primary particles are filled in a cylindrical tube separately. The method of preparing the packed bed is loose random packing; material is dropped into the bed without any pressure or vibration. Each filled bed is scanned individually by X-ray tomography. Then, a certain volume, $V_b$, at the center of the packed bed is analyzed and its void space ratio is determined by image processing (Fig. 5).

Since the definition of bulk porosity corresponds to extra void space in a bed, it is calculated as the ratio:

$$\varepsilon_b = 1 - \frac{V_{s,cp}}{V_b}. \tag{9}$$

With this definition the internal pores which belong to the primary particle structure are not considered in the bulk porosity. The resulting porosity is called the true bulk porosity in [22]. The compact solid phase volume $V_s$ can be used, instead of the porous solid phase volume $V_{s,cp}$ in Eq. (9), to calculate bulk porosity. In this case, the resulting porosity includes all pores in the bed, even internal porosity. In this work, as a reference and comparison, the bulk porosity using the compact solid volume has also been calculated. The compact solid volume is evaluated based on the number and size of foreground (white) pixels. For finding the total volume of the porous solid phase of all agglomerates, $V_{s,cp}$, first all the internal pores are filled and then the volume is calculated as in the procedure for calculating the internal porosity (Section 3.3.1).

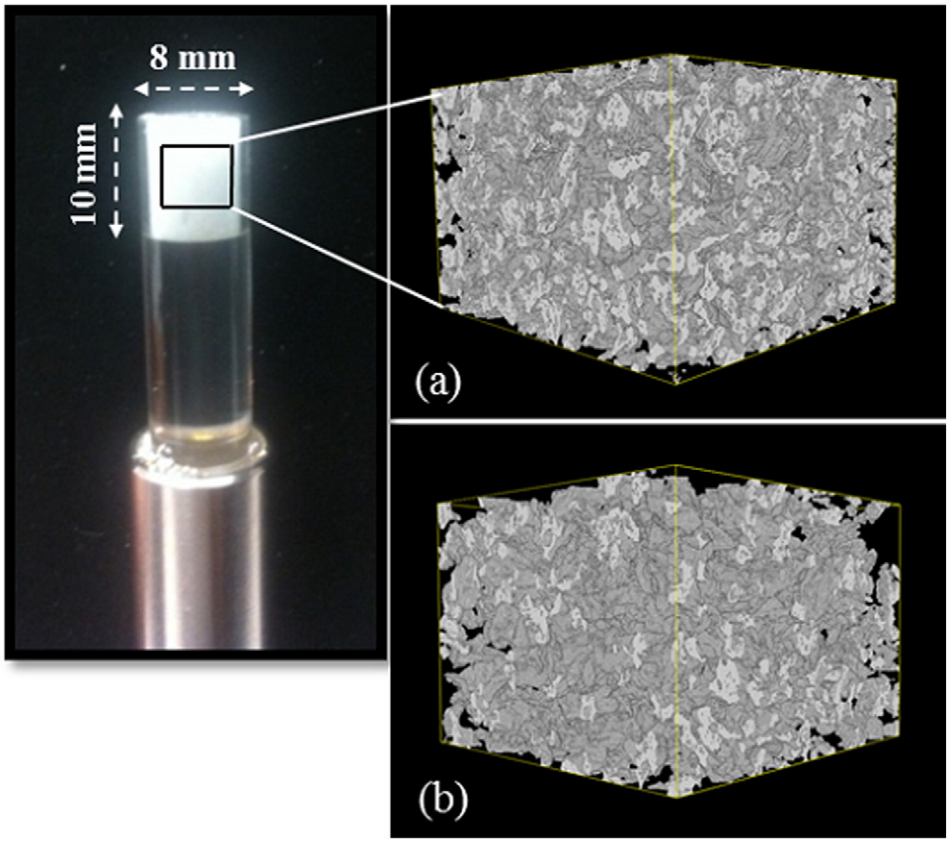


**Fig. 5.** 3D view of a maltodextrin packed bed filled with (a) primary particles and (b) agglomerates.

### 3.4. Circularity and sphericity

The circularity is commonly used in 2D shape analysis. It is defined as the degree to which the particle is similar to a circle and it is a function of the perimeter $P$ and the cross-sectional area $A$ of the agglomerate [23]:

$$C = \frac{4\pi A}{P^2}. \tag{10}$$

The required data for evaluation of circularity is obtained from measurements by the Camsizer equipment.

In three-dimensional shape analysis, the sphericity describes how closely the particle resembles a sphere. It is defined as the surface area of a sphere with the same total solid phase volume of agglomerate $V_{s,cp}$, divided by the surface area $S$ of the real 3D object [10]:

$$\phi_S = 6\sqrt{\pi}\,\frac{V_{s,cp}}{\sqrt{S^3}}. \tag{11}$$

The precision and accuracy of the volume and surface area determination are important for sphericity analysis. These quantities can be obtained from X-ray images. For spherical particles, $\phi_S$ equals unity, while for other particles it is below 1.

### 3.5. Fractal dimension

Maltodextrin agglomerates produced in a spray fluidized bed are composed of primary particles which form irregular structures. A common way to quantify this irregularity is by using the fractal dimension, which is very useful for describing shapes and the way an object fills the space, being a good measure for the structural compactness of the object. The value of fractal dimension ranges from unity for strings to three for regular three-dimensional objects, and it can have a non-integer value. If the value is about three, it means that the object has a compact structure and fills the space like a rigid sphere or cube. Agglomerates grown by particle collisions exhibit a power law scaling between the number of primary particles and radius of gyration [24]:

$$N_p = K_g\left(\frac{R_g}{\bar{r}_p}\right)^{D_f} \tag{12}$$

where the exponent $D_f$ is the fractal dimension, $\bar{r}_p$ is the mean radius of primary particles in each agglomerate, and $K_g$ is the fractal prefactor. The parameters $K_g$ and $D_f$ can be determined from a logarithmic plot of the number of primary particles $N_p$ versus the ratio $(\frac{R_g}{\bar{r}_p})$ by linear regression. This statistical scaling law can still be used to characterize agglomerates which are not strictly fractal [25,26].

## 4. Results and discussion

### 4.1. Primary particle separation and gyration radius

In the separation of primary particles with the preflooded watershed transformation (Section 3.1), the minimal pixel number has a great influence on the number of separated objects. For several values of the minimal pixel number the number of separated primary particles was determined for a series of maltodextrin agglomerates. A rough estimate

**Table 2**
The effect of the minimal pixel number in the preflooded watershed transform on the number of separated primary particles for one exemplary agglomerate.

| Minimal pixel number | 10 | 50 | 500 | 5000 | 10,000 | 12,000 | 20,000 |
|---|---|---|---|---|---|---|---|
| Number of primary particles | 42 | 22 | 14 | 9 | 5 | 5 | 4 |

for the number of primary particles is also calculated based on the volume of the porous solid phase in the agglomerate obtained from the associated X-ray images and on the median volume of the primary particles used in the agglomeration process. By comparing these two ways of determination, it can be concluded that a reasonable number of primary particles are obtained for a minimal pixel number in the range of 10,000–15,000. Table 2 shows a typical evaluation of the effect of the minimal pixel number on the number of separated primary particles in one agglomerate. Note that before the segmentation process the internal pores of the primary particles were filled because of two reasons: First, to prevent the segmentation of primary particles due to the existence of internal porosity. Second, to maintain the consistency with the rough estimation in which the total volume of primary particles, including internal porosity, is considered. The method used for the filling of the internal pores has been discussed in Section 3.3.1.

Since the primary particles are not spherical, their radii are reported in 13 discrete directions of the cuboidal lattice (3 coordinate directions, 6 face diagonals, 4 space diagonals). This data is stored in matrices for further evaluation. By approximating each primary particle by a sphere with equal volume the corresponding sphere diameter is calculated.

A 3D view of an agglomerate with primary particles separated by using different minimal pixel numbers for the segmentation is shown in Fig. 6a. Also, from the center coordinates and diameter of each primary particle, the spherical model of the agglomerate can be constructed (Fig. 6b). The polydispersity of the primary particles comprising the agglomerate is recognizable in this figure. The dispersity is overestimated for a small minimal pixel number but it decreases noticeably at higher minimal pixel number.

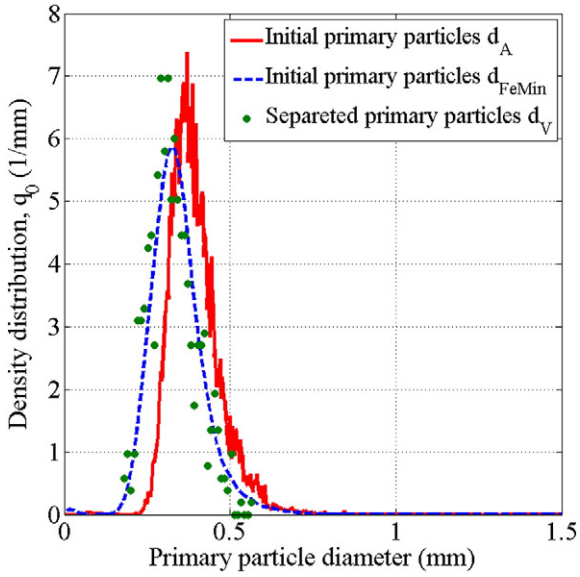


**Fig. 7.** Size distributions of primary particles obtained from μ-CT images using the segmentation method ($d_V$) and from the Camsizer ($d_A$, $d_{FeMin}$).

The watershed transform with minimal pixel number of 12,000 was used in combination with the Euclidean distance transform to separate the connected primary particles for more than 60 maltodextrin agglomerates. In order to assess the accuracy of the primary particle sizes obtained from the segmentation of the μ-CT volume images, they have

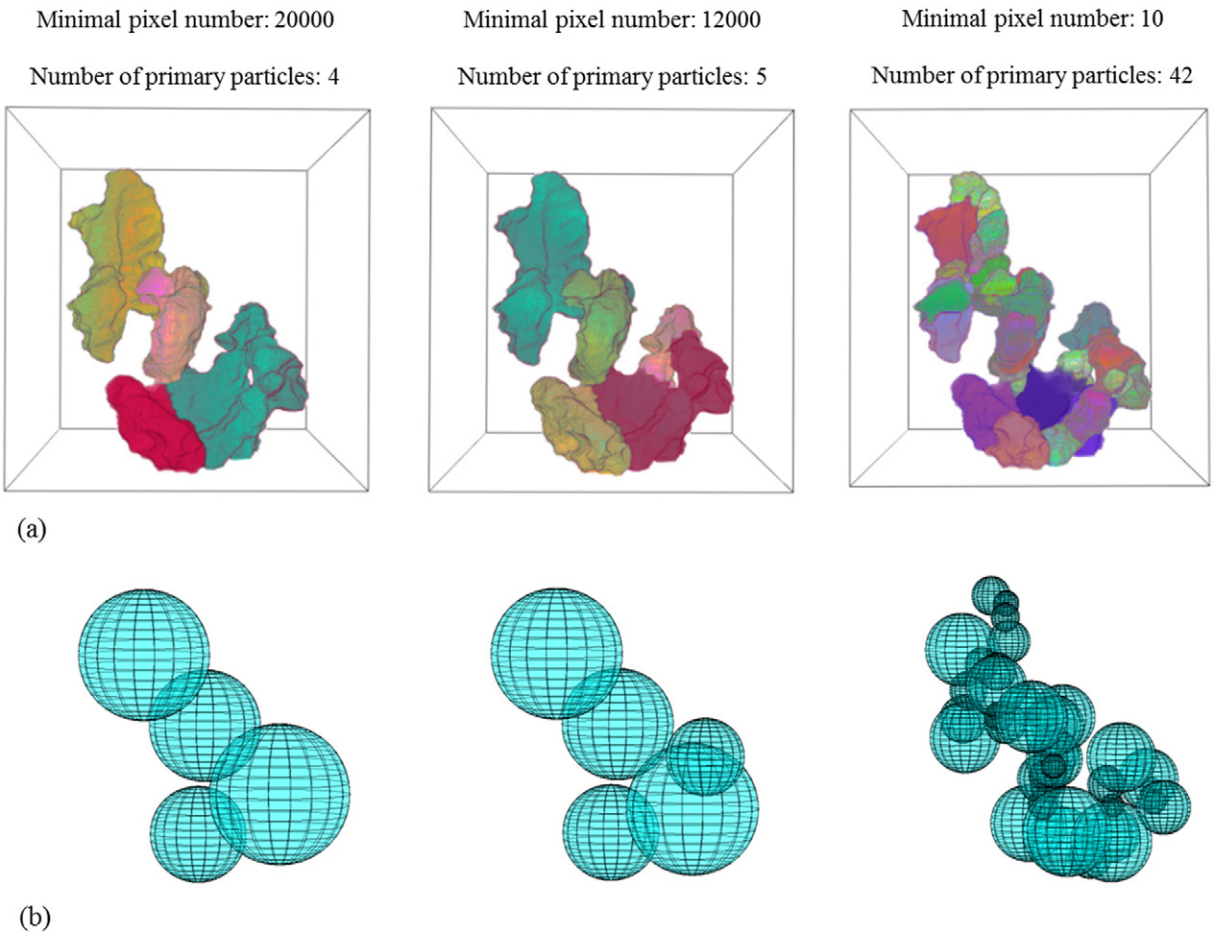


**Fig. 6.** Primary particle separation of an agglomerate for different values of the minimal pixel number: (a) real structure of primary particles, (b) approximation of each primary particle by a sphere with equal volume.

been compared with the particle size distribution before agglomeration (Fig. 7). In this comparison, the size of the separated primary particles from the X-ray images is considered as the equivalent diameter $d_V$ of spheres with equal volume. The size distribution of the primary particles before agglomeration was investigated based on their projected images by the Camsizer. Since the primary particles of maltodextrin are not spherical, their size can be represented in several ways. As the Camsizer image is not three-dimensional, for comparison with X-ray images, the size of primary particle with equal projected area, $d_A$, can be obtained first ($d_A$ is the diameter of a disk with the same area as the particle's projection). As shown in Fig. 7, there is a difference between the numbers obtained by these two methods. The particle size $d_A$ is about 13% larger than $d_V$ which is calculated from the 3D X-ray images. In principle, $d_A$ may be smaller or larger than $d_V$, depending on the particle shape and projection. However the equivalent diameter of a disk with equal area is often larger than the other equivalent diameters: Elongated particles show significantly larger values for $d_A$ than for $d_V$ [27]. Therefore, a larger value of $d_A$ compared to $d_V$ is acceptable for maltodextrin primary particles, which have an irregular shape. Another diameter used to represent the particle size in 2D is the Feret diameter. In general, it can be defined as the distance between the two parallel planes restricting the object perpendicular to a given direction in space. Minimum and maximum Feret diameters are obtained by using many such directions. According to Califice et al. [28], the diameter from 2D image analysis that best matches the true 3D size of particles is the minimum Feret diameter $d_{FeMin}$. As shown in Fig. 7, the size distribution based on $d_{FeMin}$ is in a good agreement with the $d_V$ distribution. This comparison shows that the size of the separated primary particles obtained by the segmentation method matches quite well the primary particle size distribution which was measured before the agglomeration process. It should be noted that more than a million primary particles were measured in the Camsizer, but only around 500 primary particles were separated and measured by the μ-CT device in this study.

Number ($q_0$) and volume ($q_3$) size distributions of agglomerates obtained from the Camsizer as well as the gyration diameters ($2R_g$) calculated from the μ-CT images are shown in Fig. 8. The gyration diameters of 22 agglomerates lie in five classes with size range from 0.51 to 1.24 mm and a mean value of 0.8 mm. The median value of the minimum Feret diameter $D_{FeMin}$ of agglomerates from the $q_3$ distribution is 0.642 mm. The difference between Camsizer size distributions and the radius of gyration is expected as the latter one describes not only the agglomerate size, but also how the mass is distributed around its center of gravity (see Section 3.2). It should also be noted that the samples analyzed by the Camsizer contained some agglomerated primary particles and some very fine particles which could not be separated from the original feed. The last two groups of particles result in the left-hand side branches of the Camsizer distributions in Fig. 8, but they are missing in the distribution of gyration diameter, because only agglomerates with different sizes were picked up for μ-CT analysis.

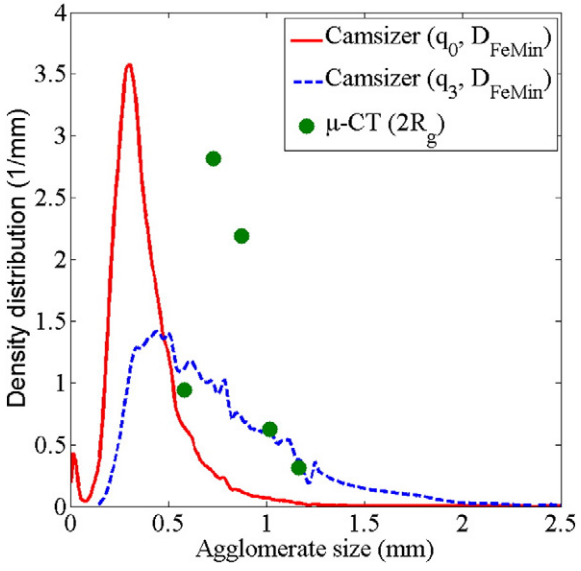


**Fig. 8.** Size distributions of agglomerates obtained from the Camsizer and of distribution of gyration diameter obtained from the μ-CT images.

### 4.2. Porosity

#### 4.2.1. Internal porosity (closed pores)

Three different structuring elements were tested for filling the small closed pores in the interior of the primary particles in the agglomerate: an approximate ball with size 3 (SE-Ball 3), a cube with size 3 (SE-Cube 3) and a cube with size 5 (SE-Cube 5). After using these three types of structuring elements for each agglomerate and after filling the larger closed pores by means of the complementing and labeling method (Section 3.3.1), the entire internal structure of the agglomerate was mapped in order to verify that all the internal closed pores were filled. In Fig. 9, the effect of the shape and size of the structuring element on the cumulative pore size distribution is illustrated. The porosity values obtained with SE-Cube 3, SE-Cube 5 and SE-Ball 3 are 8.7%, 13% and 18%, respectively. The differences in these values show the importance of choosing a suitable structuring element. After these structuring elements were applied to several different agglomerates, it was concluded that the SE-Ball 3 is the most suitable one. By this element, all the pores inside primary particles of the agglomerate are filled while the outer surface structure remains unchanged.

The average fraction of internal agglomerate pores which are not connected to the surface was found to be around 18.8%. Similar values (0.121–0.206) were reported for the internal porosity of cereal powder agglomerates in Hafsa et al. [10]. No significant difference in closed porosity values was found between the individually investigated maltodextrin agglomerates. This is because the internal porosity of agglomerates is mostly determined by the structure of the primary particles. The internal porosity of primary particles before agglomeration was found to be around 25%. This result shows that the porosity of primary particles is decreased by about 6% during agglomeration. This is because some of the internal pores are clogged by the maltodextrin substance that is dissolved in water. Moreover, in the course of the spray fluidized bed agglomeration process, the amorphous structure of maltodextrin absorbs a significant amount of water. Thus, the glass transition temperature of maltodextrin decreases strongly and the amorphous matrix undergoes a transition from the glassy to the rubbery state of

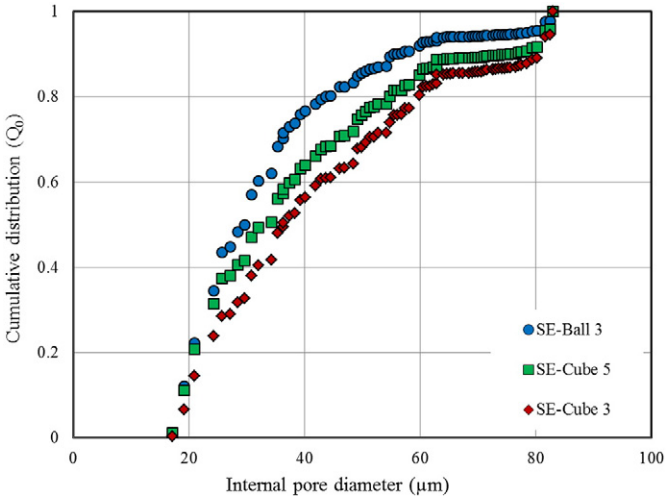


**Fig. 9.** Cumulative size distribution of closed pores in an agglomerate, obtained by the closing operator with different structuring elements as well as by the complementing and labeling methods.

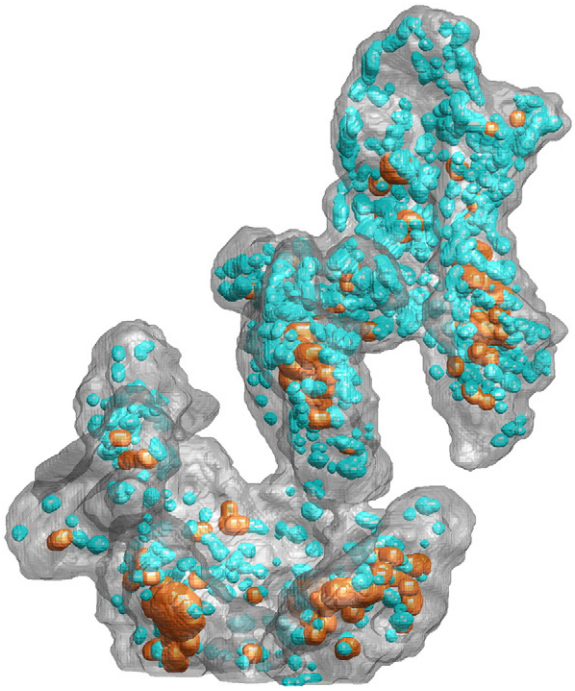

**Fig. 10.** Spatial distribution of internal pores of an agglomerate.

relatively poor dimensional stability. Consequently, this may lead to collapse of some internal pores.

The 3D view of the spatial distribution of internal pores (Fig. 10) illustrates the true internal morphology of the agglomerate. Marked with blue color are smaller pores which were defined by the closing mathematical morphology operators, while larger pores which were distinguished with the complementing and labeling method are marked in orange. The size distribution of internal pores (Fig. 11) displays pore sizes ranging between 16 and 90 μm. Moreover, in Fig. 10, the differences of pore size distributions after and before filling larger pores with the complementing and labeling methods are also shown. It should be noted that the resolution of the μ-CT images was 2.2 μm, therefore it was not feasible to detect pores smaller than 16 μm. With the closing operator (SE-Ball 3) only pores below 50 μm are identified, but after implementing the complementing and labeling methods larger

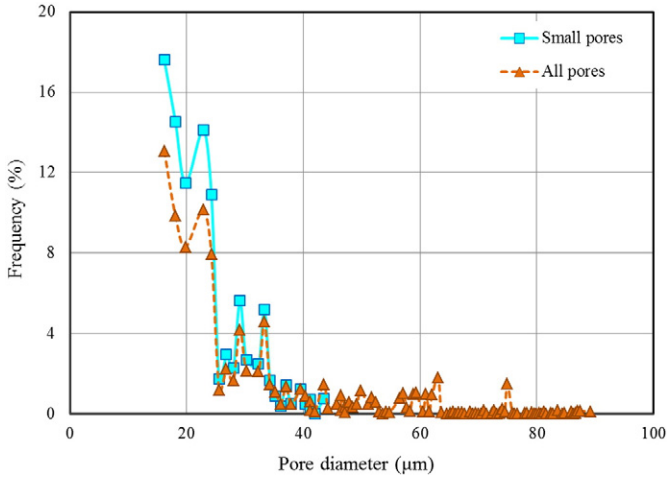


**Fig. 11.** Frequency plot of the size of internal pores in an agglomerate obtained by applying only the closing operator (small pores) or the closing operator and, additionally, the complementing and labeling methods (all pores).

pores are also distinguished. Fig. 11 is for one agglomerate with a large total number of pores and also sufficient number of pores in every size class. The same analysis was carried out for many other agglomerates with the same image analysis procedure. The results were very similar with several local minima and maxima, which are most probably related to the definition and evaluation of pores in the granulometry method. In order to reduce the analysis time, our methodology for evaluation the internal pores was also applied to packed beds of material. By this technique a significantly larger number of agglomerates or primary particles can be analyzed simultaneously. The internal porosity and the pore size range for different cases are compared in Table 3. The slightly higher values of the internal porosity obtained from the packed beds can be associated to the filling of some of the void space at the contact points during the procedure of filling the internal pores. Therefore, although with packed beds more particles are investigated in short time, the resulting porosity is by 4–5% more than the real value. One can also notice that the upper limit of the pore size range is higher in the packed bed than for single agglomerates or primary particles.

*4.2.2. Open pore porosity*

In addition to closed pores, open pores, which are connected to the surrounding air, are formed during the agglomeration process, when the primary particles stick together. Therefore, the process parameters used in the production of agglomerates are expected to have an effect on the open pore porosity.

The results for the open porosity obtained by the three different evaluation methods explained previously are plotted in Fig. 12. The comparison shows that open porosities obtained by the convex hull and the gyration radius methods are similar, whereas the open porosity obtained by the dilation method is much lower. For a complex structure with irregular shape, such as the maltodextrin agglomerate, the convex hull and the radius of gyration methods appear to be more suitable for determining the open porosity. In these methods all the channels and open cavities can be considered in the total volume, whereas in the dilation method many open pores and channels may not be covered.

The value of the open pore porosity for maltodextrin agglomerates calculated by the convex hull method is around 80%. This value is higher than the value obtained earlier for glass bead agglomerates (about 63%; Dadkhah et al. [12]). This behavior is attributed to the properties of maltodextrin being an amorphous water-soluble substance. During agglomeration, the viscosity of the residual water increases due to the dissolved amorphous substance. Therefore, sticky and plasticized surfaces of maltodextrin particles lead to the creation of more irregularly shaped agglomerates with open structures in the spray fluidized bed (Fig. 13). Since glass beads are not soluble in water and experience no glass transition during the process, the overall structure of glass bead agglomerates is more compact compared to maltodextrin agglomerates. Some agglomerates with instant properties investigated by Hogekamp et al. [29] showed open porosity values between 0.7 and 0.8 at the upper end of the particle size range, i.e., for a particle diameter of around 1 mm. Therefore, our results for open porosity with the convex hull and the gyration radius methods agree well with the values reported in [29].

*4.2.3. Bulk porosity*

In Table 3, there is a difference between bulk porosity calculated by Eq. (9) and its counterpart, which is based on the same calculation but using the compact solid volume instead of the porous solid phase volume. The difference between these two bulk porosities is linked to the internal particle porosity.

The mean bulk porosity of the primary particles is 67.6% for a packed bed of primary particles whereas it increases to 78.9% for agglomerates. The morphology and size distribution of particles has a great influence on bulk porosity [29,30]. Also, the mean value of sphericity of primary particles is larger than the agglomerate sphericity (see Table 4). Therefore, having a larger value of bulk porosity after agglomeration is

**Table 3**
Bulk and internal porosities of primary particles and agglomerates evaluated in the single particle and packed bed mode.

| Object | Internal porosity (%) | Pore diameter (μm) | Pore median diameter (μm) | Bulk porosity, based on $V_{s,cp}$ (%) | Bulk porosity, based on $V_s$ (%) |
|---|---|---|---|---|---|
| Single agglomerates[a] | 18.8 (±1.5) | 16–90 | 26.7 (±2.93) | _ | _ |
| Single primary particles[b] | 25 (±1.2) | 17–100 | 25.5 | _ | _ |
| Packed bed of agglomerates[c] | 24 | 17–115 | 25.4 | 78.9 | 82.7 |
| Packed bed of primary particles[c] | 29 | 17–143 | 24.5 | 67.6 | 75.5 |

[a] Presented values are for 5 agglomerates.
[b] Presented values are for 30 primary particles before agglomeration.
[c] Each packed bed contains at least 500 agglomerates and 3000 primary particles.

reasonable. In another study by Zou and Yu [31], the effect of particle/agglomerate shape on the bed packing has been investigated. The results therein show that the particle shape is crucial for the bed porosity, even if particles with similar sphericity are compared [22].

A lower bulk porosity (0.46–0.63) was reported in [22] for packed beds of agglomerated milk powder. It should be noted that in this work, the packing method was different and the porosity was measured after 100 taps. The packed bed of particles was, thus, more compact and the porosity lower.

Due to the irregular structure of maltodextrin agglomerates, it is not easy to find a clear relationship between the agglomerate morphology and the bulk porosity. Similar to our agglomerates, most industrially available powders show a very complex morphology. Commonly they are agglomerated to a certain degree and thereby show a large polydispersity amongst the agglomerates. The shapes of the larger agglomerates also vary widely. This generates problems when linking the particle morphology to the bulk porosity for these types of complex samples [22]. Generally, compared to spheres, the larger, less spherical agglomerates are expected to yield beds with larger porosities due to disturbances in the close packing patterns.

### 4.3. Circularity and sphericity

The circularity of the agglomerates produced in the spray fluidized bed was measured by the Camsizer for more than 2000 agglomerates which lie in 25 size classes with a width of 0.08 mm each. This measurement was repeated for three different samples and the results are shown in Fig. 14. As can be seen, the circularity generally decreases with increasing particle size, and four main regions are recognizable. Region A refers to very small particles which could not be separated from the starting material of the process. These very fine particles seem to have very high values of circularity. However, such very high values may also be related to the image resolution since the perimeter acquisition is highly resolution-dependent for small particles [32]. This would limit the ability to measure precisely the irregularity of the fine feed particles from the images acquired in the Camsizer and lead to an overestimation of the circularity according to Eq. (10). Once the size range of unagglomerated primary particles has been reached, a plateau in the graph is observed (region B) and the circularity remains rather constant until the size of small agglomerates (~0.4 mm) has been attained. Then for intermediate agglomerates (region C), a clear trend of decreasing circularity with increasing agglomerate size is visible. In the agglomeration process, after a while these intermediate agglomerates stick together and secondary agglomeration occurs. Therefore, the circularity increases noticeably for agglomerates with a size of about 1 mm. After that, again by increasing the size of secondary agglomerates, the circularity decreases slightly (region D). Maltodextrin spray fluidized bed agglomeration in two stages is also reported in Avilés-Avilés et al. [4].

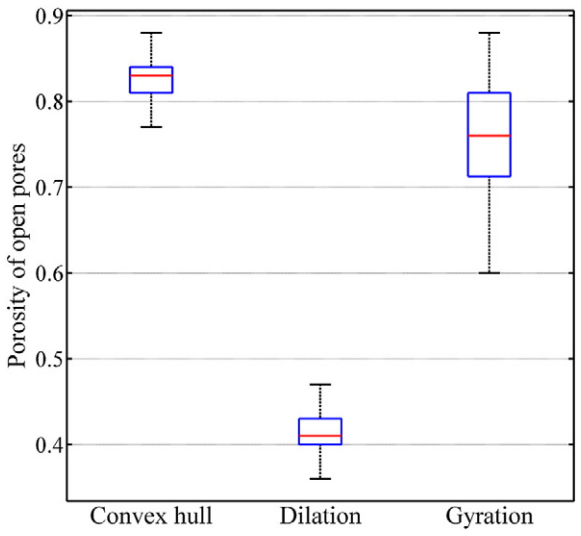


**Fig. 12.** The open pore porosity of agglomerates, determined by three different methods.

The sphericity of the agglomerates was measured from the 3D reconstructed X-ray images (Fig. 15). The results are compared with the 2D Camsizer image results in Table 4. The mean sphericity value of agglomerates obtained from the X-ray images is 0.19. Similar values of sphericity (0.20–0.23) were reported by Hafsa et al. [10] for laboratory grains produced under low shear conditions along with higher values (0.41–0.45) for industrial grains produced under high shear conditions. Moreover, even higher values of sphericity (0.78–0.87) were reported for granules produced in a twin screw extruder by Lee et al. [33]. In the present work, the overall trend of agglomerate sphericity (Fig. 15) is similar to the trend of the circularity results (Fig. 14). The sphericity decreases with the agglomerate size, but remains significantly smaller than the circularity. The differences in these results may be due to image resolution. Circularity measurement in the Camsizer can probably not fully consider the surface irregularity of the agglomerates, so that the overall shape of the agglomerates appears to be more spherical than the real structure. Moreover, the analysis of single randomly-selected 2D projections clearly leads to incomplete results. It is not yet clear how many projections of an irregular agglomerate are needed in order to guarantee reliable characterization of its size and shape [23].

As illustrated in Fig. 15 and Table 4, an increase in sphericity is observed by applying the dilation morphological operator with a certain structuring element (SE-Ball 3) on the X-ray images. By implementing the dilation method, the small scale structural irregularity is diminished and the results become more compatible with the 2D Camsizer images. Increasing the size of the structuring element to SE-Ball 5 leads to a higher degree of filling of the pores and cavities, and to values closer to the circularity from the Camsizer. However, the 3D image analysis without manipulation may still be expected to more closely reflect the true physical shape of the agglomerates. Although the 2D image analysis yields a similar trend and requires less time and labor, the circularity values seem to be overestimated by about 50% compared to the sphericity values.

In general, 2D structural properties can be easily obtained from projected image analysis, however 3D parameters such as volume, surface area and sphericity need more sophisticated instruments (e.g. X-ray micro-computed tomography) that are more time consuming and in most cases cannot be applied to a large number of agglomerates.

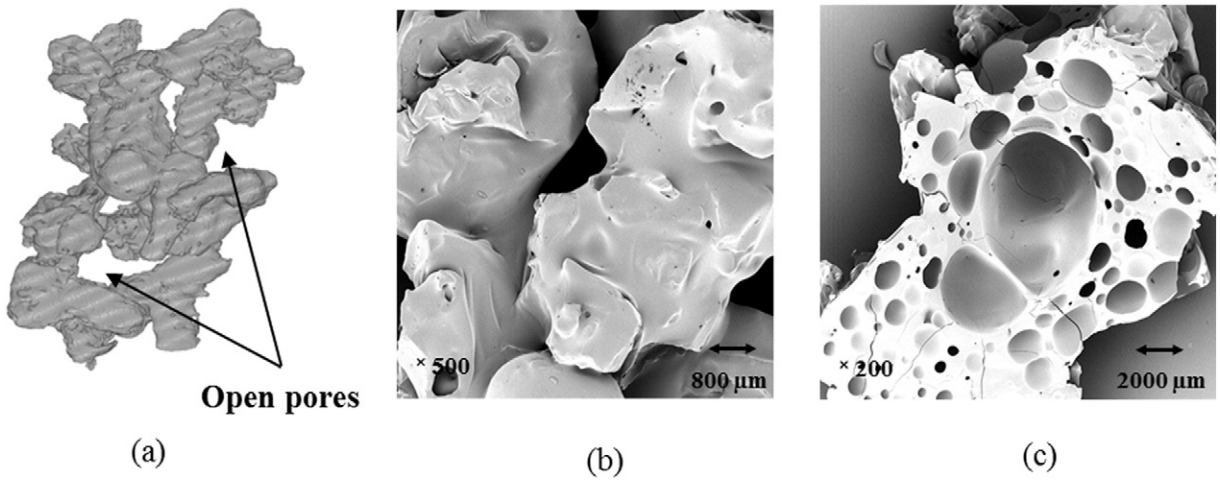


**Fig. 13.** Maltodextrin agglomerate: (a) overall 3D view illustrating the irregular structure of the agglomerate with open pores (X-ray image), (b) plasticized surfaces after agglomeration (REM image), (c) cross-sectional view showing the small and large internal pores (REM image).

Many studies can be found in the literature that explore the possibility of obtaining 3D parameters from 1D and 2D variables [34–37]. However, a comprehensive investigation on this subject is still missing, since most of the previous studies did not measure 3D parameters directly and/or their relationships with 1D and 2D properties were not analyzed in detail. It is also reported in [23] that out of all the correlations found for estimating 3D parameters from 1D and 2D variables, those related to sphericity have the highest average errors. It can be concluded that sphericity is a challenging parameter to be estimated from 2D variables.

### 4.4. Fractal dimension

The logarithmic representation of Eq. (12) for a series of agglomerates is depicted in Fig. 16. As can be seen, linearity is fulfilled with a good accuracy. Therefore, the maltodextrin agglomerates produced in fluidized bed can be considered as fractal-like, i.e., they satisfy Eq. (12) even though they are not self-similar over many length scales. The values of the fractal dimension and the pre-factor are $D_f = 1.81$ and $K_g = 1.04$, respectively. The low value obtained for the fractal dimension in this research illustrates the non-compact and fluffy structure of maltodextrin agglomerates. As reported by Eggersdorfer et al. [38], $D_f$ of around 1.8 or 1.9 corresponds to the open structure of aerosol fractal-like particles which were generated by diffusion-limited mechanism. During sintering, the value of $D_f$ increases up to 3 when the particles become fully compacted. The same work illustrates the usefulness of fractal dimension in describing the change in structure for a process that starts with aggregates consisting of several hundreds of primary particles and ends up with just one large spherical object. The fractal dimension of glass bead agglomerates, which were produced in the same spray fluidized bed at similar process conditions, was reported to be in the range of 2.09–2.94 [39]. The smaller fractal dimension of maltodextrin agglomerates compared to the relatively compact glass bead agglomerates is an expected result. Also, in contrast to glass bead agglomerates, maltodextrin agglomerates consist of primary particles with different sizes, as shown in Fig. 6. It is pointed out in Eggersdorfer and Pratsinis [24] and Eggersdorfer et al. [38] that low fractal dimension of agglomerates can be attributed to primary particle polydispersity. Broadening the primary particle size distribution of the agglomerates decreases monotonically their $D_f$, and for a sufficiently broad distribution (standard deviation > 2.5) the $D_f$ reaches about 1.5 regardless of the collision mechanism [24].

**Table 4**
Values for sphericity and circularity of primary particles and agglomerates.

| Particles/method | Sphericity/circularity |
|---|---|
| Primary particles/2D Camsizer images | 0.60 (±0.021) |
| Agglomerates/2D Camsizer images | 0.37 (±0.06) |
| Agglomerates/3D X-ray images[a] | 0.19 (±0.027) |
| Agglomerates/3D X-ray images + dilation (SE-Ball 3)[a] | 0.24 (±0.033) |
| Agglomerates/3D X-ray images + dilation (SE-Ball 5)[a] | 0.36 (±0.041) |

[a] Presented values are for 25 agglomerates.

### 4.5. General discussion

In this study, efforts have been undertaken to describe in detail the morphological features of maltodextrin agglomerates produced in a spray fluidized bed by X-ray 3D imaging. The question arises, which advantages this sophisticated characterization method would have in terms of its ability to provide morphological data that can be used for assessment, modeling or simulation of product properties when compared to conventional characterization techniques. This shall be briefly discussed in the present section, along with some remarks on structure–property relations and on merits and limitations of 3D imaging and conventional characterization methods.

An important application property of particulate products is their ability to withstand storage without loss of quality. During storage, hygroscopic products of biological origin that can undergo glass transition (such as maltodextrin) are in danger of sintering [40]. Moisture uptake from the atmosphere reduces significantly the glass transition temperature, so that the product may become rubbery at ambient conditions

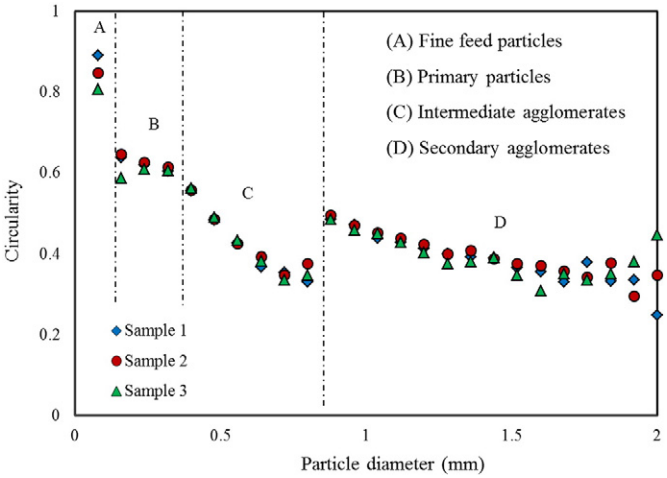


**Fig. 14.** Circularity of particles after agglomeration measured by Camsizer.

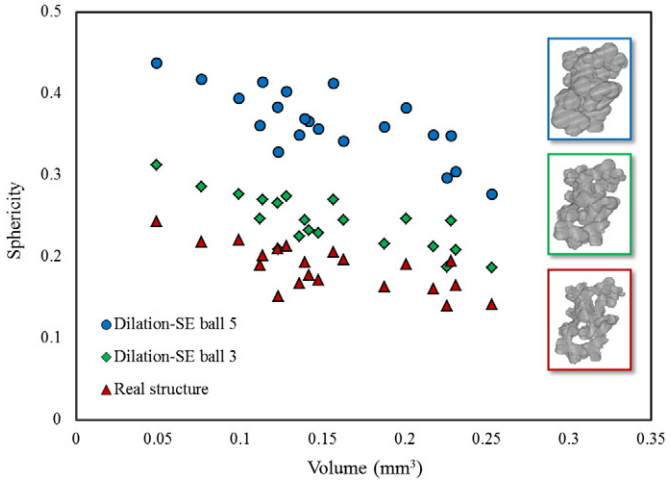


**Fig. 15.** Sphericity of different agglomerates evaluated from 3D X-ray images with the real structure and with structures modified by the dilation method.

and sinter, which would completely destroy its whole user property profile. The most advanced models and scaling laws presently available for agglomerate sintering come for aerosol science and refer to flame produced nanoparticle aggregates [24,38,41]. The key morphological descriptor contained in them is, as already indicated, the fractal dimension of the aggregates, which controls and expresses both, the rate of the sintering process and the change of morphology during this process. However, fractal dimension is not accessible by any conventional characterization method, so that 3D imaging and the method, which has been introduced in the present work for identification of primary particles, are indispensable for future application of those models and also to agglomerates made of bigger particles.

Apart from sintering and the activity of nanoparticles, the morphology of aerosol and colloidal agglomerates, expressed by fractal dimension and the radius of gyration, is known to affect their hydrodynamic properties, specifically their mobility diameter and, in consequence, scattering, suspension and precipitation behavior [26]. The precipitation behavior of agglomerates produced in a spray fluidized bed in water and

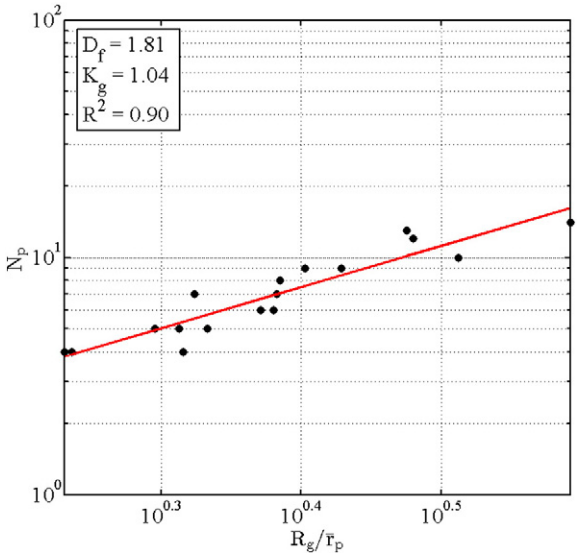


**Fig. 16.** Number of primary particles per agglomerate vs. the normalized radius of gyration.

their movement in the fluidizing air during the production process are expected to depend on morphology in a similar way. The former is essential for instant product properties (i.e. fast dissolution), the latter (via interparticle collision frequency) for the rate of the spray fluidized bed process. Since the key background morphological descriptors are not accessible by conventional methods, characterization by 3D imaging is, again, crucial for future exploration and better understanding of these effects.

Another important application property of agglomerated material is the mechanical strength of the agglomerates. Early simplistic models correlate strength with just the open porosity of agglomerates, stating that the mechanical strength increases with decreasing open pore porosity [40]. However, newer and better performing models make use of the number of primary particles in the agglomerate, the coordination number for the contacts of primary particles with each other, and the strength of contact bonds [40,42]. Alternatively, discrete simulation methods can be applied, namely the discrete element method (DEM) [42,43]. It is very clear that neither advanced models for agglomerate strength nor DEM simulations can be conducted on the basis of conventional characterization methods, because such methods simply cannot provide the necessary information about morphology. In contrast, all necessary morphological data are provided by X-ray μ-CT. To these belong the number of primary particles, grace to the method introduced for primary particle identification, and primary particle coordination number, which is easy to evaluate after the primary particles have been identified, though not explicitly discussed in this paper. Moreover, X-ray μ-CT provides full data for the morphology of individual agglomerates (including the bonds between primary particles), so that the DEM could be applied on real agglomerate structures (including respective statistics), instead of reconstructing numerically agglomerate structures from previously selected or identified morphological descriptors [42].

The list of structure dependent application properties can be arbitrarily expanded. For example, the bulk porosity of agglomerated powder is known to affect the stress and flow behavior in storage, handling and transportation equipment [44]. Properties such as rehydration, dissolution, and disintegration of agglomerates in water also depend on the presence and type of pores. For dry food agglomerates, the rehydration ratio and moisture diffusivity increase with the bulk and open pore porosities as these pores allow for a quick penetration of water into the particle matrix and thus wetting phenomena occur faster [14,45]. Good dispersion of agglomerated powder in the liquid is necessary in order to achieve an efficient reconstitution with limited lump formation, presupposing an efficient wetting of the porous bed, which relates to bed structure and void space [45–47]. In all these cases the same arguments hold as previously discussed: Conventional characterization methods can give some hints about structure–property relationships, but they cannot provide the detailed information needed in order to apply or develop sophisticated and new methods for modeling or simulating such relationships.

To further point out the limitations of conventional characterization methods let us return to the example of agglomerate strength and assume that this can be unequivocally and uniquely correlated with porosity, as the earliest models for agglomerate strength imply. Even then, mercury porosimetry, i.e. the standard method for the determination of porosity and pore size distribution, would not provide reliable input data in case of instant agglomerates for two main reasons. Firstly, because of the shape and structure of maltodextrin (or similar) agglomerates, it is eventually impossible to determine the intrusion starting point [14]. This is due to the fact that the pores and cavities are of similar size as the void space between agglomerate particles. Therefore, the results from mercury porosimetry are considered to be more representative of the bulk porosity, whereas μ-CT can measure the porosity of any single agglomerate. Secondly, instant agglomerates are often docile and fragile, so that they can be compacted or damaged during mercury porosimetry. Moreover, mercury porosimetry cannot detect closed

pores and uses a model in order to derive structural information from the primary measurement result, whereas X-ray μ-CT relies directly on the distribution of different phases in space. The limitations of mercury porosimetry have been quantitatively pointed out in [11].

Concerning the size of agglomerates (in its traditional definitions) conventional measuring techniques are well established. However, particle shape is also important for the properties of particulate products, for example bed porosity [22], and enormously variable in food powders and agglomerates, which range from extreme irregularity (grinded materials such as spices and sugar) to approximate sphericity (starch and dried yeast) or well-defined crystal shapes (granulated sugar and salt) [48]. 2D image analysis gives only partial information about the particle shape, whereas 3D image analysis allows for the measurement of true particle characteristics [28]. Hence, 3D shape data can be used to discuss the accuracy of other methods. In this study, the shape (and also the size) of particles was investigated in both, two and three dimensions with the Camsizer and X-ray μ-CT, respectively, and the results were compared. On these grounds, two lines of future development are seen in this field: To develop correlations between 3D shape results (which require time-consuming X-ray μ-CT to be retrieved) and 2D shape results (which are easier and faster to obtain); to better delineate the adequacy and applicability of 2D or 3D shape results for computation of application properties.

Despite its discussed known and potential advantages, X-ray μ-CT can only be conducted on a limited number of agglomerates, a lot less than the thousands of particles analyzed by traditional size measurement techniques or the number of agglomerates usually analyzed by mercury porosimetry. However, it is not the number of investigated agglomerates that counts in terms of statistical significance in some cases, but the much higher number of other and smaller structural elements, for example the number of primary particles or closed pores for the respective size distributions (Figs. 7 and 11). In the case of internal porosity and sphericity of single agglomerates measured by the μ-CT, small standard deviations were obtained, with values of $\pm 1.5\%$ and $\pm 0.027$, respectively (see Tables 3 and 4). The internal porosity and circularity values obtained for the primary particles had standard deviations of merely $\pm 1.2\%$ and $\pm 0.021$, respectively. These small standard deviations indicate that the amount of samples analyzed here represents the properties of the whole population of particles quite reliably. Concerning the reliability in the determination of fractal properties, Dadkhah and Tsotsas [39] asked the question by how much the fractal dimension originally determined for about 28 agglomerates would change by considering a significantly smaller number of agglomerates. To answer this question, they randomly picked half of the agglomerates from the original sample and determined again the value of $D_f$. Forty realizations of this procedure resulted in a small standard deviation and in a mean value very close to the value of $D_f$ previously determined for the original, large sample.

## 5. Conclusion and outlook

The present work provided a comprehensive characterization of the internal structure of maltodextrin agglomerates produced in spray fluidized bed by means of X-ray microtomography. This technique gave the opportunity to completely visualize and quantify the internal structure of such agglomerates in 3D at scales down to the micron level. Then, by a series of image processing steps performed on the X-ray images, the porosity of single agglomerates was calculated in terms of closed pores and open pores. The bulk porosity of the packed bed was also investigated for maltodextrin particles before and after agglomeration. The sphericity of maltodextrin agglomerates with an irregular structure was calculated based on the volume and surface area obtained from the 3D X-ray images. Sphericity was compared to the circularity of agglomerates obtained from an analysis of 2D images acquired by a Camsizer. The rather large difference of these two values was first explained by differences in the image resolution between the two techniques. Second, for irregular particles, the 2D image analysis gives only partial information on the shape, whereas 3D image analysis allows the measurement of the true characteristics of the particles.

The separation of the primary particles of maltodextrin with a non-spherical shape was done by an improved preflooded watershed segmentation method. In order to separate the primary particles of the agglomerate in a reasonable way, the suitable minimal pixel number was found for this kind of agglomerates, which exhibit a complex structure. Based on the information obtained from separated primary particles, the radius of gyration and the fractal dimension were calculated for a series of agglomerates. The low value of the fractal dimension, the high value of the porosity and the low value of the sphericity proved that maltodextrin agglomerates produced in a spray fluidized bed exhibit an irregular, open and fluffy structure.

The present work demonstrates the ability of the X-ray μ-CT method to describe the 3D morphology and the internal microstructure of food agglomerates. The most serious limitation concerns the time and effort necessary for measurement and, especially, for image processing, which limits the number of agglomerates that can be analyzed and assessed.

In the future, for higher accuracy and for comparison, the radius of gyration and fractal dimension will be calculated for the real structure of the agglomerate from the voxel coordinates and voxel gray values of 3D X-ray images. Also, the values and the behavior of the evaluated morphological descriptors will be presented and discussed for agglomerates produced at different process conditions. In this work, the long term vision is to link the morphology of particulate materials with the process conditions on one side and with their end-user properties (e.g. strength, flowability, compressibility, instant properties) on the other side. The presented morphological characterization is an essential step along this path.

## Abbreviations

| | |
|---|---|
| μ-CT | micro-computed tomography |
| SE-Ball 3 | structuring element; shape: approximate ball, size: 3 |
| SE-Ball 5 | structuring element; shape: approximate ball, size: 5 |
| SE-Cube 3 | structuring element; shape: cube, size: 3 |
| SE-Cube 5 | structuring element; shape: cube, size: 5 |

## Acknowledgments

This work was conducted in the frame of the graduate school "Micro–Macro-Interactions in Structured Media and Particle Systems" (GRK 1554), funded by the Deutsche Forschungsgemeinschaft (DFG). The X-ray μ-CT device was financed by the EFRD, European Fund for Regional Development (project no. 1211080002). The maltodextrin powder was kindly provided by the Roquette Company.

## References

[1] S. Palzer, Agglomeration of pharmaceutical, detergent, chemical and food powders: similarities and differences of materials and processes, Powder Technol. 206 (2011) 2–17, http://dx.doi.org/10.1016/j.powtec.2010.05.006.
[2] K. Terrazas-Velarde, M. Peglow, E. Tsotsas, Kinetics of fluidized bed spray agglomeration for compact and porous particles, Chem. Eng. Sci. 66 (2011) 1866–1878, http://dx.doi.org/10.1016/j.ces.2011.01.037.
[3] M. Hussain, J. Kumar, E. Tsotsas, Modeling aggregation kinetics of fluidized bed spray agglomeration for porous particles, Powder Technol. 270 (2015) 584–591, http://dx.doi.org/10.1016/j.powtec.2014.07.015.
[4] C. Avilés-Avilés, E. Dumoulin, C. Turchiuli, Fluidised Bed Agglomeration of Particles With Different Glass Transition Temperatures, Powder Technol, 2014, http://dx.doi.org/10.1016/j.powtec.2014.03.026.
[5] D. Dopfer, S. Palzer, S. Heinrich, L. Fries, S. Antonyuk, C. Haider, A.D. Salman, Adhesion mechanisms between water soluble particles, Powder Technol. 238 (2013) 35–49, http://dx.doi.org/10.1016/j.powtec.2012.06.029.
[6] L. Ziyani, N. Fatah, Use of experimental designs to optimize fluidized bed granulation of maltodextrin, Adv. Powder Technol. 25 (2014) 1069–1075, http://dx.doi.org/10.1016/j.apt.2014.02.013.
[7] L. Fries, S. Antonyuk, S. Heinrich, G. Niederreiter, S. Palzer, Product Design Based on Discrete Particle Modeling of a Fluidized Bed Granulator, Particuology, 2014, http://dx.doi.org/10.1016/j.partic.2013.10.004.

[8] L. Fries, S. Antonyuk, S. Heinrich, D. Dopfer, S. Palzer, Collision dynamics in fluidised bed granulators: a DEM–CFD study, Chem. Eng. Sci. 86 (2013) 108–123, http://dx.doi.org/10.1016/j.ces.2012.06.026.
[9] R. Pyrz, Application of X-ray Microtomography to the Study of Polymer Composites, 1999, http://dx.doi.org/10.4271/1999-01-5614.
[10] I. Hafsa, B. Cuq, S.J. Kim, A. Le Bail, T. Ruiz, S. Chevallier, Description of internal microstructure of agglomerated cereal powders using X-ray microtomography to study of process–structure relationships, Powder Technol. 256 (2014) 512–521, http://dx.doi.org/10.1016/j.powtec.2014.01.073.
[11] N. Rahmanian, M. Ghadiri, X. Jia, F. Stepanek, Characterisation of granule structure and strength made in a high shear granulator, Powder Technol. 192 (2009) 184–194, http://dx.doi.org/10.1016/j.powtec.2008.12.016.
[12] M. Dadkhah, M. Peglow, E. Tsotsas, Characterization of the internal morphology of agglomerates produced in a spray fluidized bed by X-ray tomography, Powder Technol. 228 (2012) 349–358, http://dx.doi.org/10.1016/j.powtec.2012.05.051.
[13] D.R. Baker, L. Mancini, M. Polacci, M.D. Higgins, G.A.R. Gualda, R.J. Hill, M.L. Rivers, An introduction to the application of X-ray microtomography to the three-dimensional study of igneous rocks, Lithos 148 (2012) 262–276, http://dx.doi.org/10.1016/j.lithos.2012.06.008.
[14] L. Farber, G. Tardos, J.N. Michaels, Use of X-ray tomography to study the porosity and morphology of granules, Powder Technol. 132 (2003) 57–63, http://dx.doi.org/10.1016/S0032-5910(03)00043-3.
[15] N. Otsu, A threshold selection method from gray-level histograms, IEEE Trans. Syst. Man Cybern. 9 (1) (1993) 62–66.
[16] A. Bleau, L.J. Leon, Watershed-based segmentation and region merging, Comput. Vis. Image Underst. 77 (2000) 317–370, http://dx.doi.org/10.1006/cviu.1999.0822.
[17] P. Tahmasebi, M. Sahimi, Reconstruction of nonstationary disordered materials and media: watershed transform and cross-correlation function, Phys. Rev. E 91 (2015) 1–11, http://dx.doi.org/10.1103/PhysRevE.91.032401.
[18] L.J. Belaid, W. Mourou, Image segmentation: a watershed transformation algorithm, Image Anal. Stereol. 28 (2009) 93–102, http://dx.doi.org/10.5566/ias.v28.p93-102.
[19] J. Ohser, K. Schladitz, 3D Images of Materials Structures: Processing and Analysis, John Wiley & Sons, Inc., New York, 2009.
[20] I. Teraoka, Polymer Solution: An Introduction to Physical Properties, John Wiley & Sons, Inc., New York, 2002.
[21] C. Ratti, Advances in Food Dehydration, Taylor & Francis Group, Boca Raton, 2009.
[22] E. Börjesson, F. Innings, C. Trägårdh, B. Bergenståhl, M. Paulsson, Evaluation of particle measures relevant for powder bed porosity — a study of spray dried dairy powders, Powder Technol. 253 (2014) 453–463, http://dx.doi.org/10.1016/j.powtec.2013.11.050.
[23] G. Bagheri, C. Bonadonna, I. Manzella, P. Vonlanthen, On the Characterization of Size and Shape of Irregular Particles, 2702015 141–153, http://dx.doi.org/10.1016/j.powtec.2014.10.015.
[24] M.L. Eggersdorfer, S.E. Pratsinis, The structure of agglomerates consisting of polydisperse particles, Aerosol Sci. Technol. 46 (2012) 347–353, http://dx.doi.org/10.1080/02786826.2011.631956.
[25] U. Koeylue, Y. Xing, D.E. Rosner, Fractal morphology analysis of combustion generated aggregates using angular light scattering and electron microscope images, Langmuir 11 (1995) 4848–4854, http://dx.doi.org/10.1021/la00012a043.
[26] A.D. Melas, L. Isella, A.G. Konstandopoulos, Y. Drossinos, Morphology and mobility of synthetic colloidal aggregates, J. Colloid Interface Sci. 417 (2014) 27–36, http://dx.doi.org/10.1016/j.jcis.2013.11.024.
[27] H.G. Merkus, Particle Size Measurements Fundamentals, Practice, Quality, Springer, 2008.
[28] A. Califice, F. Michel, G. Dislaire, E. Pirard, Influence of particle shape on size distribution measurements by 3D and 2D image analyses and laser diffraction, Powder Technol. 237 (2013) 67–75, http://dx.doi.org/10.1016/j.powtec.2013.01.003.
[29] S. Hogekamp, M. Pohl, Porosity measurement of fragile agglomerates, Powder Technol. 130 (2003) 385–392, http://dx.doi.org/10.1016/S0032-5910(02)00240-1.
[30] E. Tsotsas, Heat and mass transfer in packed beds with fluid flow, VDI Heat Atlas, 10th ed.Springer, Berlin/Heidelberg, Germany 2010, pp. 1327–1341.
[31] R.P. Zou, A.B. Yu, Evaluation of the packing characteristics of mono-sized non-spherical particles, Powder Technol. 88 (1996) 71–79, http://dx.doi.org/10.1016/0032-5910(96)03106-3.
[32] M. Zeidan, X. Jia, R.A. Williams, Errors implicit in digital particle characterisation, Chem. Eng. Sci. 62 (2007) 1905–1914, http://dx.doi.org/10.1016/j.ces.2006.12.011.
[33] K.T. Lee, A. Ingram, N.A. Rowson, Comparison of granule properties produced using twin screw extruder and high shear mixer: a step towards understanding the mechanism of twin screw wet granulation, Powder Technol. 238 (2013) 91–98, http://dx.doi.org/10.1016/j.powtec.2012.05.031.
[34] D. Asahina, M.A. Taylor, Geometry of irregular particles: direct surface measurements by 3-D laser scanner, Powder Technol. 213 (2011) 70–78, http://dx.doi.org/10.1016/j.powtec.2011.07.008.
[35] S.J. Blott, K. Pye, Particle shape: a review and new methods of characterization and classification, Sedimentology 55 (2008) 31–63, http://dx.doi.org/10.1111/j.1365-3091.2007.00892.x.
[36] M.A. Taylor, E.J. Garboczi, S.T. Erdogan, D.W. Fowler, Some properties of irregular 3-D particles, Powder Technol. 162 (2006) 1–15, http://dx.doi.org/10.1016/j.powtec.2005.10.013.
[37] E.J. Garboczi, X. Liu, M.A. Taylor, The 3-D shape of blasted and crushed rocks: from 20 μm to 38 mm, Powder Technol. 229 (2012) 84–89, http://dx.doi.org/10.1016/j.powtec.2012.06.012.
[38] M.L. Eggersdorfer, D. Kadau, H.J. Herrmann, S.E. Pratsinis, Aggregate morphology evolution by sintering: number and diameter of primary particles, J. Aerosol Sci. 46 (2012) 7–19, http://dx.doi.org/10.1016/j.jaerosci.2011.11.005.
[39] M. Dadkhah, E. Tsotsas, Influence of process variables on internal particle structure in spray fluidized bed agglomeration, Powder Technol. 258 (2014) 165–173, http://dx.doi.org/10.1016/j.powtec.2014.03.005.
[40] M. Peglow, S. Antonyuk, M. Jacob, S. Palzer, S. Heinrich, E. Tsotsas, Particle formulation in spray fluidized beds, in: E. Tsotsas, A.S. Mujumdar (Eds.), Modern Drying Technology: Product Quality and Formulation, vol. 3, Wiley-VCH, Weinheim 2007, pp. 295–378.
[41] M.L. Eggersdorfer, D. Kadau, H.J. Herrman, S.E. Pratsinis, Multiparticle sintering dynamics: from fractal-like aggregates to compact structures, Langmuir 27 (2011) 6358–6367, http://dx.doi.org/10.1021/la200546g.
[42] R. Moreno-Atanasio, M. Ghadiri, Mechanistic analysis and computer simulation of impact breakage of agglomerates: effect of surface energy, Chem. Eng. Sci. 61 (2006) 2476–2481, http://dx.doi.org/10.1016/j.ces.2005.11.019.
[43] A. Hassanpour, S.J. Antony, M. Ghadiri, Modelling of agglomerate behavior under shear deformation: effect of velocity field of a high shear mixer granulator on the structure of agglomerates, Adv. Powder Technol. 18 (2007) 803–811, http://dx.doi.org/10.1163/156855207782515094.
[44] R.A. Williams, M.S. Beck, Process Tomography: Principles, Techniques and Applications, first ed. Butterworth-Heinemann, Oxford, 1995.
[45] A. Marabi, I.S. Saguy, Effect of porosity on rehydration of dry food particulates, J. Sci. Food Agric. 84 (2004) 1105–1110, http://dx.doi.org/10.1002/jsfa.1793.
[46] H. Schubert, Instantization of powdered food products, Int. Chem. Eng. 33 (1993) 28–45.
[47] E. Ortega-Rivas, Bulk properties of food particulate materials: an appraisal of their characterisation and relevance in processing, Food Bioprocess Technol. 2 (2009) 28–44, http://dx.doi.org/10.1007/s11947-008-0107-5.
[48] G.V. Barbosa-Cánovas, E. Ortega-Rivas, P. Juliano, H. Yan, Food Powders: Physical Properties, Processing, and Functionality, Kluwer Academic/Plenum Publishers, New York, 2005.